The Actuator Line Model in Lattice Boltzmann Frameworks: Numerical Sensitivity and Computational Performance

IOP Conf. Series: Journal of Physics: Conf. Series **1256** (2019) 012022 doi:10.1088/1742-6596/1256/1/012022

The Actuator Line Model in Lattice Boltzmann Frameworks: Numerical Sensitivity and Computational Performance

Henrik Asmuth, Hugo Olivares-Espinosa, Karl Nilsson, Stefan Ivanell

Uppsala University, Wind Energy Section, Campus Gotland, 621 67 Visby, Sweden

E-mail: henrik.asmuth@geo.uu.se

Abstract. The growing use of large-eddy simulations for the modelling of wind farms makes the need for efficient numerical frameworks more essential than ever. GPU-accelerated implementations of the Lattice Boltzmann Method (LBM) have shown to provide significant performance gains over classical Navier-Stokes-based computational fluid dynamics. Yet, their use in the field of wind energy remains limited to date. In this fundamental study the cumulant LBM is scrutinised for actuator line simulations of wind turbines. The numerical sensitivity of the method in a simple uniform inflow is investigated with respect to spatial and temporal resolution as well as the width of the actuator line's regularisation kernel. Comparable accuracy and slightly better stability properties are shown in relation to a standard Navier-Stokes implementation. The results indicate the overall suitability of the cumulant LBM for wind turbine wake simulations. The potential of the LBM for future wind energy applications is clarified by means of a brief comparison of computational performance.

1. Introduction

The aerodynamic interaction of wind turbines has attained growing interest due to the increasing significance of wind power for today's power systems. A wide range of model fidelities is being developed and used in the field today [1]. The highest model fidelity refers to Large-Eddy Simulations (LES) fully resolving the large energy-containing scales of the transient flow field of wind turbine wakes. However, their use comes at an immense computational cost when compared to low-fidelity models and even RANS [2]. Still, an increasing availability of computational resources has made LES a feasible approach for the study of wind energy related flow problems, even including simulations of entire wind farms [3]. Naturally, earlier LES studies focused on the understanding of the method itself, for instance in conjunction with actuator models [4, 5]. In recent years, though, LES are also used in more applied contexts, such as the investigation of fatigue loads [6, 7], turbine curtailment [3, 8] or farm-wide optimisation control strategies [9]. Despite the growing capacities of modern High-Performance Computing (HPC) clusters, computational demand remains the biggest bottleneck. One way to increase computational performace, is the use of a different numerical approach, namely the Lattice Boltzmann Method (LBM). Orignially evolving from lattice gas cellular automata [10], the LBM today states a powerful alternative to classical CFD approaches. Besides the method's excellent parallelisability, its numerical simplicity, suitability for complex geometries and multiphase flows have led to a wide adoption in both academia and industry [11, 12]. Moreover, the strict

locality of the computationally intense steps of the scheme render the LBM perfectly suitable for implementations on graphics processing units (GPUs). Speed-up factors when compared to single-node LBM-CPU implementations are commonly found as 100 and more [13, 14] and multi-GPU implementations can be considered as the state-of-the-art in lattice Boltzmann computing [15, 14]. Yet, to date, only a few studies have shown applications of the LBM in the field of atmospheric boundary layer (ABL) flows and wind energy. Such is, for instance, the work of Deiterding and Wood [16], who presented promising results of geometrically resolved wind turbines. Others presented investigations of large-scale urban flows as shown in [17, 18].

As a first step to scrutinise the LBM for LES of wind farms, this study shall provide an investigation of the actuator line model (ALM) in lattice Boltzmann frameworks. Again, investigations of actuator models in general and specifically the ALM in the LBM are still limited. To our best knowledge, the 2D-ALM for vertical axis turbines by Rullaud et al. [19] currently states the only example. Thorough numerical analyses of the ALM as found in classical Navier-Stokes (NS) frameworks [20, 5, 21, 22] are thus inevitable for the future use of the LBM in this field. In this paper we provide an initial numerical sensitivity analysis of the ALM in a lattice Boltzmann framework. Using the cumulant LBM, the interplay of spatial and temporal resolution with the smearing width is investigated in terms of resulting blade forces along the Actuator Line (AL) as well as near-wake properties. Also, an exemplary performance comparison to a state-of-the-art AL implementation in a NS framework is presented further motivating the use of GPU-accelerated LB frameworks in the field of wind energy.

2. The Lattice Boltzmann Method

The governing equation of the LBM is the kinetic Boltzmann equation describing the time evolution of particle distribution functions (PDF) f. More specifically, f states the probability to encounter a particle (mass) density of velocity $\boldsymbol{\xi}$ at time t at location $\boldsymbol{x}$. Discretising the Boltzmann equation in physical and velocity space we obtain the lattice Boltzmann equation (LBE) without external forces

$$f_\alpha(t + \Delta t, \boldsymbol{x} + \Delta t\, \boldsymbol{e}_\alpha) - f_\alpha(t, \boldsymbol{x}) = \Omega_\alpha \quad , \tag{1}$$

with $\boldsymbol{e}_\alpha$ denoting the particle velocity in a discrete lattice direction α while the collision operator Ω_α on the RHS models the redistribution of f through particle collisions within the control volume. The crucial aspect of the LBM is the discretisation of the velocity space by means of a velocity lattice. Common lattices for three-dimensional problems are the D3Q19 and the D3Q27 with 19 and 27 lattice directions, respectively. Also note that, here, the lattice velocity c is chosen such that $c = \Delta x/\Delta t$. PDFs are hereby inherently advected to the next lattice node during one time step, explaining the simplicity of eq. (1). Furthermore, dimensional analysis yields the macroscopic mass density and momentum as the zeroth- and first-order raw velocity moment of f, respectively, i.e.

$$\rho(t, \boldsymbol{x}) = \sum_{\alpha=1}^{m} f_\alpha(t, \boldsymbol{x}) \quad , \quad \rho \boldsymbol{u}(t, \boldsymbol{x}) = \sum_{\alpha=1}^{m} \boldsymbol{e}_\alpha\, f_\alpha(t, \boldsymbol{x}) \tag{2}$$

As the LBE states a compressible formulation, incompressibility requires simulations at the low Mach number limit $\mathrm{Ma} \ll 1$. With the lattice speed of sound $c_s = c/\sqrt{3}$ the pressure is then given as $p = \rho/3$. Further selected aspects of the LBM will be given in the following. For more fundamentals the interested reader is referred to the comprehensive work by Krüger et al. [12].

2.1. Scaling and Accuracy of the LBM

In order to fulfil with the aforementioned requirements of the LBE physical units need to be rescaled to non-dimensional lattice units (hereafter indexed $(\cdot)^{LB}$), i.e. $c = \Delta x^{LB}/\Delta t^{LB} = 1$.

Hence, scaling factors C for all relevant physical units can be derived via non-dimensional quantities namely Re and Ma. Within this study we shall define the Reynolds number as $\mathrm{Re}_D = u_0\, D/\nu$, where u_0 is the inflow velocity and D the turbine diameter. The Mach number is consequently given by u_0 and the speed of sound: $\mathrm{Ma} = u_0/c_s$. Starting from the spatial scaling factor we obtain $C_x = \Delta x/\Delta x^{LB} = L_i/n_i$, where L_i is the length of the (sub-)domain and n_i the number of grid points in the referring spatial dimension. With $c_s^{LB} = c/\sqrt{3}$, the reference velocity on the lattice is given by $u_0^{LB} = Ma/\sqrt{3}$, yielding the velocity scaling factor $C_u = \sqrt{3}\, u_0/Ma$. It follows that the temporal scaling factor is given by $C_t = C_x/C_u$, which implies a physical time step $\Delta t = C_t\, \Delta t^{LB}$ that is inherently proportional to the grid spacing and Mach number.

A formal error analysis of the LBM is arguably cumbersome, especially for highly non-linear problems where truncation terms beyond leading order need to be considered [12]. As a reminder, to leading order the spatial and temporal discretisation error scales with Δx^2 and Δt^2, respectively. Additionally, the Chapman-Enskog analysis yields the so called compressibility error occurring as an additional term $\mathcal{O}((u^{LB})^3)$ in the macroscopic stress tensor and therefore scaling with Ma^2. The LBM thus only recovers the NS solution with second order in space under so called diffusive scaling, i.e. $\Delta t \propto \Delta x^2$. Following from the above, Ma should thus be refined proportionally to Δx. When only reducing Δx the increasing compressibility error can even become dominant and deteriorate spatial convergence. Mind that this again implies a formal reduction to first-order in time.

2.2. The Cumulant Collision Model

Until today, various collision models of different complexity have been suggested. The most widely adopted, yet also the most simple, is the single relaxation time model (SRT), commonly referred to as lattice Bhatnagar-Gross-Kroog (LBGK) model [23]. In the SRT model, all PDFs are relaxed towards an equilibrium state using a single constant relaxation time τ. The collision operator then reads

$$\Omega_\alpha = -\frac{\Delta t}{\tau}\left(f_\alpha - f_\alpha^{eq}\right) = -\frac{\Delta t}{\tau} f_\alpha^{neq} \quad , \tag{3}$$

where f_α^{eq} is obtained from the second-order Taylor expansion of the Maxwellian equilibrium. Via Chapman-Enskog expansion of the LBE it can be shown that

$$\tau = \frac{1}{\omega} = 3\nu/c^2 + \Delta t/2 \quad , \tag{4}$$

with ν being the shear viscosity [24].

Poor numerical stability of the SRT model led to the development of multiple-relaxation-time models (MRT), see for instance [25, 26]. In MRT models pre-collision PDFs are transformed into a velocity moment space. Each individual moment is then relaxed towards a referring equilibrium with an individual relaxation time and subsequently transformed back into particle distribution space. An increased stability when compared to the SRT can thus be achieved by calibrating the relaxation times of non-hydrodynamic moments [26, 27]. Still, several aspects of the MRT render the model unsuitable for the use at high Reynolds numbers as required for studies of wind turbines. Such are, among others, the lack of a universal formulation for optimal collisions rates and deficiencies stemming from the rather arbitrary choice of moment space, lacking Galiliean invariance and the introduction of hyper-viscosities [28]. Preliminary tests of this study confirmed the insufficiency of the MRT for such high Reynolds numbers. The flow field appeared highly degenerated by reflections of spurious oscillations originating in regions of high velocity gradients. Only higher spatial resolutions could remedy this issue. This, however, can be considered impractical for future wind farm applications. The MRT is thus not further investigated as part of this paper.

To overcome the issues of the MRT, Geier et al. [28] suggested a more universal formulation based on independent observable quantities of the PDFs, i.e., cumulants. First, PDFs are transformed into frequency space using the two-sided Laplace-transform

$$F(\boldsymbol{\Xi}) = \mathcal{L}\left(f(\boldsymbol{\xi})\right) = \int_{-\infty}^{\infty} f(\boldsymbol{\xi})\, e^{-\boldsymbol{\Xi}\cdot\boldsymbol{\xi}} d\boldsymbol{\xi} \quad , \tag{5}$$

with $\boldsymbol{\Xi} = \{\Xi, \Upsilon, Z\}$ denoting the wave number space of the particle velocity $\boldsymbol{\xi} = \{\xi, \upsilon, \zeta\}$. Countable cumulants $c_{\alpha\beta\gamma}$ can then be written as

$$c_{\alpha\beta\gamma} = c^{-\alpha-\beta-\gamma} \frac{\partial^\alpha \partial^\beta \partial^\gamma}{\partial\Xi^\alpha \partial\Upsilon^\beta \partial Z^\gamma} \ln\left(F(\Xi, \Upsilon, Z)\right) \quad . \tag{6}$$

After the transformation, the cumulants are again relaxed towards the referring equilibrium in cumulant space. Throughout this study all relaxation rates of higher-order cumulants are set to one, commonly reffered to as AllOne cumulant. The higher-order cumulants are hereby instantly relaxed towards the equilibrium providing an inherently stable solution. Yet, note, that a parametrisation of the relaxation rates might be preferable in terms of accuracy [29, 30]. An investigation thereof in this context is left for future reference. Also note, that cumulants as defined in eq. (6) can be efficiently computed via central velocity moments of f [28, 31]. As opposed to raw moments as given in eq. (2) and used in many MRT models, the moment space then refers to a moving frame of reference with velocity $\boldsymbol{u}$. Hence, body forces F, can simply be incorporated by shifting the frame of reference by

$$\boldsymbol{u} = \boldsymbol{u} + \frac{\Delta t}{2\,\rho} \boldsymbol{F} \quad , \tag{7}$$

2.3. Large-eddy Simulations in Lattice Boltzmann Frameworks

With growing maturity of the LBM, LES approaches have attained increasing attention over the last decade. Commonly, eddy-viscosity approaches like the standard Smagorinsky [32] as well as dynamic approaches [33] are adopted and incorporated using eq. (4). In this study no explicit SGS model is applied. The inherently stable AllOne-cumulant LBM is thereby applied as an underresolved DNS or implicit LES, respectively. Despite lacking theoretical evidence of implicit SGS characteristics of the collision operator, such use is in line with various preceding promising studies [34, 35, 14]. Moreover, the influence of the SGS model on the ALM itself (in uniform inflow) is generally small, as found by Sarlak et al. [36] using similar spatial resolutions. For future investigations on the far-wake of the turbine though, it will obviously be of specific interest.

3. Numerical Framework

The investigation of the ALM will be based on simulations of the NREL 5MW reference turbine [37] in uniform inflow of $u_0 = 8\mathrm{m\,s^{-1}}$, similar to preceding studies, see [50, 22]. The turbine is set to operate at a tip-speed-ratio $\lambda = 7.55$ referring to the point of optimal power production. With the viscosity of air $\nu = 1.78 \cdot 10^{-5}\mathrm{m^2\,s^{-1}}$ the Reynolds number of the case amounts to $\mathrm{Re}_D = 5.7 \cdot 10^7$. Details regarding the utilised solvers and numerical set-up are given in the following.

3.1. The Lattice Boltzmann Solver elbe

The lattice Boltzmann computations are performed using the GPU-based efficient lattice Boltzmann environment elbe[1] [38] mainly developed at Hamburg University of Technology (TUHH). The implementation of the cumulant LBM in elbe was recently validated in a comprehensive study by Gehrke et al. [35].

[1] `https://www.tuhh.de/elbe`

3.2. EllipSys3D

As a finite-volume (FV) NS reference we consult the well-established multi-purpose solver EllipSys3D developed at the Technical University of Denmark (DTU) by Michelsen [39, 40] and Sørensen [41]. The code has been applied to numerous wind power related flow problems and served for several fundamental investigations of the ALM [20, 42, 5, 36].

3.3. The Actuator Line Model

The investigated ALM follows the well-documented standard procedures as given in [20, 5, 43] and others. Rotor forces are determined using the relative velocity u_{rel} of the referring blade elements along the AL. These are computed from the locally sampled velocity components using

$$u_{rel} = \sqrt{u_n^2 + (\Omega\, r - u_\theta)^2} \quad , \tag{8}$$

where u_n is the velocity in blade-normal (streamwise) direction, u_θ is the tangential velocity component, Ω the rotational velocity of the turbine and r the radial position of the blade element. The local blade forces per unit length read

$$\boldsymbol{F} = 0.5\,\rho\, u_{rel}^2\, c\,(C_L \boldsymbol{e}_L + C_D \boldsymbol{e}_D) \quad . \tag{9}$$

Here, ρ is the fluid density and c the chord length. The lift and drag coefficients C_L and C_D, respectively are obtained from tabulated airfoil data as functions of the local angle of attack and Reynolds number. The resulting forces are subsequently distributed in space in a three-dimensional Gaussian manner by taking the convolution integral of $\boldsymbol{F}$ with a regularisation kernel η_ϵ, given by

$$\eta_\epsilon = \frac{1}{\pi^{3/2}\,\epsilon^2}\, e^{-(d/\epsilon)^2} \quad , \tag{10}$$

where ϵ adjusts the width of the regularisation and d is the distance to the centre of the referring blade element. For the sake of simplicity, a constant smearing width $\epsilon(r)$ is applied throughout this entire study. Herewith, we aim for a general understanding of of the LB-ALM that can serve as a guideline for future applications using more sophisticated approaches, see e.g. [44].

3.4. Case Set-up

The numerical set-up of the LBM and the FV-NS reference (referred to as LB-ALM and NS-ALM, respectively) are kept as similar as possible in order to ensure the best comparability possible. Certain differences though remain inavoidable due to the inherently different underlying numerical concepts. The overall rectangular domain measures 15 rotor diameters D in the streamwise direction x and $10\,D$ in the lateral directions y and z. The rotor is laterally centred $5\,D$ downstream of the inlet. In both set-ups the finest grid level with uniform grid spacing Δx_f extends from $1\,D$ upstream of the turbine to $7\,D$ downstream and comprises $3\,D$ in both lateral directions. In the LB-ALM a nested grid-refinement approach following Filippova and Hänel [45] is applied. The innermost grid region is nested in a coarser region with $2\Delta x_f$ which again is nested in the outermost grid region with $4\Delta x_f$. In the NS-ALM the grid is uniformly stretched from the inner equidistant region towards the outer domain boundary. Note that normal and tangential blade forces showed negligible changes when increasing the extent of the inner grid region. Differences in the area of interest (the innermost grid region) arising from the different refinement approaches are therefore ruled out. At the lateral boundaries a slip boundary condition is applied. A simple anti-reflecting extrapolation boundary condition [28] is used at the outlet in the LBM set-up. Statistics are gathered over a period of two domain flow-through times after an initial run-up of the same length. Results obtained from a stand-alone BEM method (see [46] for a detailed description) will be used as a reference for the resulting blade forces along the AL.

4. Numerical Sensitivity Analysis and Verification

The accuracy of blade forces obtained from an ALM is a close interplay of the solution of the flow field and the width of the regularization kernel ϵ. On the one hand, it was shown that a small ϵ is generally desirable for the correct reproduction of tip vortices [4] as well as optimal induction properties in terms of the resulting body forces [47]. On the other hand, the lower limit of ϵ is usually set by the stability of the numerical scheme [5, 48, 21]. Another requirement of the ALM is a temporal resolution that is fine enough for the blade tip not to skip a cell during one time step. As for NS approaches, this usually implies a CFL number small enough for the NS solution to become independent of Δt, see Troldborg et al. [5]. As for the LBM, the scaling laws outlined in section 2.1 suggest that the ALM time step requirement is inherently met since low Mach numbers usually dictate a Δt far below the critical value. Still, it would be naive to assume time independence of the overall solution, chiefly due to the compressibility error. As opposed to most NS studies, the numerical sensitivity of the LB-ALM thus needs to be scrutinised in terms of smearing width, spatial *and* temporal discretisation, where the latter is commonly used interchangeably with the choice of Mach number since $\Delta t \propto \mathrm{Ma}$.

4.1. Interaction of Mach Number and Smearing Width

As a starting point three different smearing widths at four Mach numbers are investigated using a spatial resolution of $\Delta x = 1/64\,D$. Resulting mean normalised body forces are given in fig. 1. At $\epsilon = 3\Delta x$, both the NS- and the LB-ALM show acceptable agreement with the

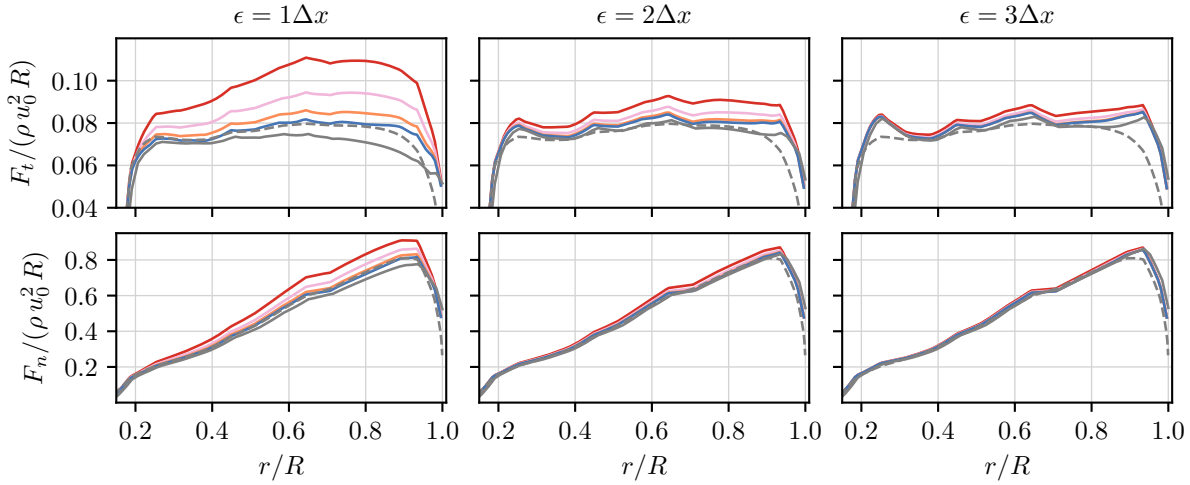

Figure 1: Mean blade forces in the tangential (F_t) and normal (F_n) direction along the AL using different smearing widths ϵ. LB-ALM at Ma = 0.1 (——), Ma = 0.05 (——), Ma = 0.025 (——), Ma = 0.0125 (——), NS-ALM (——), BEM ref. (- - -).

BEM reference. The largest discrepancies are found near the tip as well as the root for the tangential force. These discrepencies can be expected, largely because of the three-dimensional regularisation kernel. This leads to forces being smeared beyond the blade tip and root. Also, the force projection of individual blade elements eventually overlaps with neighbouring projections [44]. Furthermore, the sampled velocity is affected by the velocity induction of the trailing vortices as recently shown by Meyer-Forsting et al. [49]. The LB-ALM also shows a small Mach number dependency, yet differences towards the NS-ALM decrease with Ma. As expected, the fit with the BEM reference improves using $\epsilon = 2\Delta x$. The Mach number dependency of the LB-ALM is found significantly higher which mostly shows in the tangential force component. Note, referring to preceding studies $\epsilon = 2\Delta x$ states the lower limit for colocated FV approaches

before instabilities start to deteriorate the solution [5, 48, 21]. The NS-ALM results at $\epsilon = 1\Delta x$ can therefore be expected. The mean body forces deviate severely from the BEM reference. Likewise, the scatter in the time signal of the resulting forces increases by about one order of magnitude, measured in terms of the standard deviation of the signal. As for the LB-ALM, severe deviations from the reference are found for Ma=0.1 but again converge towards the BEM reference when decreasing its value. Even though deteriorations of the flow field could not be observed, the scatter in the forces was also increased when compared to larger ϵ. Further tests in more realistic inflows including turbulence will have to show if the severity of this scatter is acceptable for future applications.

Above all, this initial test series shows the general suitability of the cumulant LBM for AL simulations. At sufficiently low Mach numbers and common choices for the smearing width ($\epsilon \geq 2\Delta x$) the method behaves similarly to the standard FV-NS approach. Moreover, it is shown that the use of smaller values for ϵ is generally possible, yet requiring lower Mach numbers. As this increases computational cost, larger ϵ might remain preferable for future applications if one is not specifically interested in features of the tip vortices. Fundamentally, the described behaviour illustrates the effects of high-magnitude locally-applied body forces on the accuracy of the LBM. For each respective ϵ in this test series, differences in the resulting blade forces must be dominated by a decreasing compressibility error as we only decrease the Mach number. Then again lowering ϵ, the magnitude of the locally applied body forces and hence momentum increases. The compressibility error thereby becomes higher than at larger values of ϵ as it scales with $\mathcal{O}((u^{LB})^3)$. This again can explain the increasing Mach number dependency with decreasing ϵ.

4.2. Spatial resolution

Next, the effect of spatial resolution on the LB-ALM is investigated. We therefore compare three spatial resolutions using the smearing widths $\epsilon = \{1/16, 1/8\}\, D$. The LB simulations are scaled diffusively which according to section 2.1 implies $\mathrm{Ma} \propto \Delta x$. Also, two starting points are considered ($\mathrm{Ma}_0 = \{0.1, 0.05\}$), meaning that we alter the Mach number at the coarsest spatial resolution. For the sake of conciseness, all results are presented in terms of mean thrust and power coefficient, C_T and C_P, see fig. 2. At $\epsilon = 1/16\, D$ the LB-ALM shows significantly

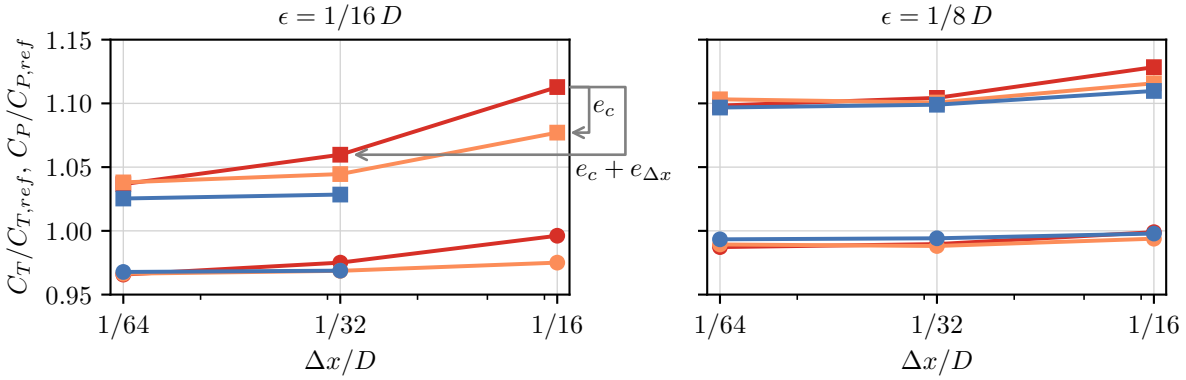

Figure 2: Mean thrust and power coefficients normalised by BEM reference values ($C_{T,ref} = 0.86$, $C_{P,ref} = 0.55$). LB-ALM starting from with $\mathrm{Ma}_0 = 0.1$, C_T: ● , C_P: ■ . LB-ALM with $\mathrm{Ma}_0 = 0.05$, C_T: ● , C_P: ■ . NS-ALM, C_T: ● , C_P: ■ .

higher errors for low spatial resolutions than the NS reference. This again does appear almost grid-independent for all considered resolutions. The discrepancy between LB and NS does, however, decrease if the initial Mach number is reduced. While this overall trend can similarly

be observed for $\epsilon = 1/8\,D$ it is far less pronounced. By means of the exemplary annotation in fig. 2 we can relate these findings to section 4.1. Under diffusive scaling both the compressibility error e_c and the discretisation error $e_{\Delta x}$ decrease simultaneously. Only decreasing Ma though, purely reduces e_c whereas $e_{\Delta x}$ remains unaffected. The comparison of the two thus reveals the dominant role of the former. Based thereupon, we can conclude that the smaller differences between low and high resolutions for $\epsilon = 1/8\,D$ primarily relate to a generally lower e_c. From a more practical point of view it should be stressed that under diffusive scaling differences in C_P and C_T change less than 1% for $\Delta x < \epsilon/4$ as similarly found for this NS-ALM and others [21]. Grid independence in that sense is thus found at similar scales as in NS frameworks. A similar dependency on the grid resolution can be seen for the velocity deficit in the near-wake as shown in fig. 3. In both frameworks, differences between $\Delta x = 1/32\,D$ and $\Delta x = 1/64\,D$ as

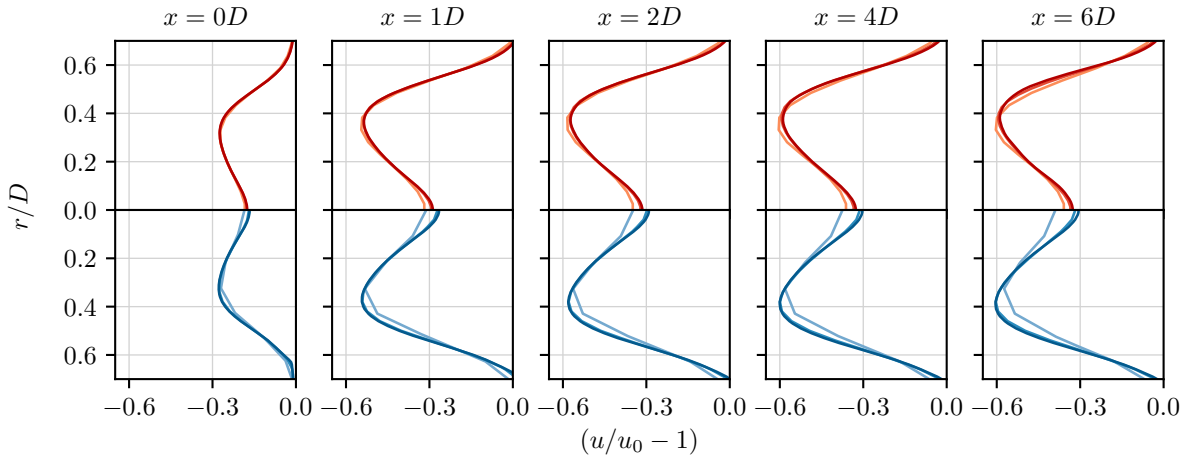

Figure 3: Wake velocity deficit at different cross-sections downstream with $\epsilon = 1/8\,D$. LB-ALM with $\Delta x = 1/16\,D$, Ma = 0.1 (—), $\Delta x = 1/32\,D$, Ma = 0.05 (—), $\Delta x = 1/64\,D$, Ma = 0.025 (—). NS-ALM with $\Delta x = 1/16\,D$ (—), $\Delta x = 1/32\,D$ (—), $\Delta x = 1/64\,D$ (—).

well as between the two approaches are very small. The largest deviation is found in the center of the wake. This, however, rather seems to relate to small differences in the computation of the near-root blade forces (not shown here) than the solution of the bulk flow. To sum up, the overall agreement of all compared parameters lies well within the scope of uncertainties of similar code-to-code comparisons [50, 36]. Further studies of the far-wake including a comparison of turbulence statistics are obviously inevitable to complement the fundamental analysis of the LB-ALM. Yet, these will be published elsewhere, due to the brevity of this paper.

5. Computational Performance

A number of comprehensive performance analyses of GPU-LB implementations can be found in the literature, see, e.g. [13, 15, 14]. Here, we refrain from such and rather provide a practical comparison for wind energy applications using the cases presented in this work. After all, with the utilized domain sizes and use of an ALM these cases can be seen as representative for many similar applications. For instance, the simple (structured) grid including a local refinement would similarly be found in typical ABL simulations. Generally, we shall consider the NS-ALM as the baseline for this comparison. The smaller time step and slightly larger grid employed in the LBM are therefore seen as an inherent overhead that has to be accepted. The process time per flow-through time (referring to 236s of physical time) therefore states the most significant performance measure. Additionally, the performance in MNUPS (million node updates per

second) is provided, which is more common for LB applications. Obviously though, the latter can not explicitly depict the aforementioned overhead.

Table 1: Performance measures of both ALM implementations at $\Delta x = 1/64D$ (as dicussed in section 4.2) using EllipSys3D and elbe, respectively. Wall time and process time given per flow-through time.

	EllipSys3D	elbe
Processing unit	1024 CPU cores (Intel Xeon Gold 6130)	1 GPU (Nvidia GTX 1080 Ti)
Grid nodes	$33.5 \cdot 10^6$	$35 \cdot 10^6$
CFL number	0.102	0.014
Mach number	-	0.025
Wall time [h]	2.74	0.86
Process time [CPUh,GPUh]	2804.30	0.86
Performance in MNUPS	32.14	560.82

As seen in table 1, the LBM case ran in about a third of the wall time when compared to the NS reference. Or, in other words, despite a significantly lower time step, a higher computational performance was achieved a single GPU (on a desktop PC) than on a large allocation on an HPC cluster. Evidently, in both frameworks the wall time could be further reduced by increasing paralellisation. In that regard, the difference in process time which is of $\mathcal{O}(10^3)$ appears more meaningful. It gives an idea of the hardware required to achieve a similar performance in a classical NS CPU-based framework when compared to a GPU-based LB implementation. In line with other studies in the field, this brief comparison again highlights the high potential of GPU-accelerated LB simulations. Also note, that latest works on this matter even report real-time computations of ABL flows on domains with $\mathcal{O}(10^9)$ grid points [52]. Regardless of performance, for future wind energy applications the use of multiple GPUs might generally be inevitable. This relates to the fact that the maximal amount of computable grid nodes is inherently bound by the internal memory of the utilised cards, a general bottleneck of GPU-implementations. The 12 GB of this GPU are apparently fully occupied by a case of this grid size.

6. Conclusion

In this paper we demonstrated the general feasibility of wind turbine simulations using the ALM in LB frameworks. It is shown that the cumulant LBM, in contrast to other collision operators, provides a suitable bulk scheme for the simulation of wind turbines using the ALM at full-scale Reynolds numbers. As expected from theory [28], the method showed no sign of numerical instability in the turbulent wake despite the high Reynolds number and rather low spatial resolutions. It thereby fulfils a crucial requirement for future wind farm simulations. Higher spatial resolutions than tested in this study would imply unacceptably large numbers of grid points for such applications. Also, high-magnitude local body forces and associated sharp velocity gradients of the ALM do not cause stability issues and provide comparable results to the Navier-Stokes-based ALM. Generally, good agreement was found in terms of blade forces and the near-wake velocity deficit between the LB-ALM and a NS reference solution. In that sense the model can be seen as successfully verified. Future analyses will have to determine its capabilities to model the turbulent far-wake. Prior applications of the cumulant LBM to highly-turbulent flows are in any way promising, see [34, 29]. Moreover, the computational performance of the method was illustrated using an exemplary test case. A fixed interval of physical time was simulated in a comparable wall time on one off-the-shelf consumer graphics card using the

LBM as on 1024 CPU cores on an HPC cluster using a state-of-the-art finite volume Navier-Stokes approach. Based on this and other studies we can conclude that the cumulant LBM is a promising approach to facilitate LES of wind turbines at a fraction of the usual computational demand.

Acknowledgements
The authors would like to thank Christian F. Janßen and Martin Gehrke (TUHH) for the many fruitful discussions regarding the cumulant LBM. Also, the support of Niels N. Sørensen and Niels Troldborg (DTU) is highly appreciated. EllipSys3D simulations were performed on resources provided by the Swedish National Infrastructure for Computing (SNIC) at NSC.

References

[1] Sanderse B, van der Pijl S and Koren B 2011 *Wind Energy* **14** 799–819
[2] Mehta D, van Zuijlen A, Koren B, Holierhoek J and Bijl H 2014 *J. Wind Eng. Ind. Aerodyn.* **133** 1 – 17
[3] Nilsson K, Ivanell S, Hansen K S, Mikkelsen R, Sørensen J N, Breton S P and Henningson D 2015 *Wind Energy* **18** 449–467
[4] Ivanell S, Sørensen J N, Mikkelsen R and Henningson D 2009 *Wind Energy* **12** 63–80
[5] Troldborg N, Sørensen J N and Mikkelsen R 2010 *Wind Energy* **13** 86–99
[6] Nebenführ B and Davidson L 2017 *Wind Energy* **20** 1003–1015
[7] Meng H, Lien F S and Li L 2018 *Renewable Energy* **116** 423 – 437
[8] Dilip D and Porté-Agel F 2017 *Energies* **10**
[9] Munters W and Meyers J 2018 *Energies* **11**
[10] McNamara G and Zanetti G 1988 *Phys. Rev. Lett.* **61**(20) 2332–2335
[11] Malaspinas O and Sagaut P 2014 *J. Comput. Phys.* **275** 25 – 40
[12] Krüger T, Kusumaatmaja H, Kuzmin A, Shardt O, Silva G and Viggen E M 2016 *The Lattice Boltzmann Method - Principles and Practice* (Heidelberg, Germany: Springer)
[13] Schönherr M, Kucher K, Geier M, Stiebler M, Freudiger S and Krafczyk M 2011 *Comput. Math. Appl.* **61**
[14] Onodera N and Idomura Y 2018 *Supercomputing Frontiers* ed Yokota R and Wu W (Springer International Publishing) pp 128–145
[15] Obrecht C, Kuznik F, Tourancheau B and Roux J J 2013 *Comput. Math. Appl.* **65** 252 – 261
[16] Deiterding R and Wood S L 2016 *J. Phys.: Conf. Series* **753** 082005
[17] King M F, Khan A, Delbosc N, Gough H L, Halios C, Barlow J F and Noakes C J 2017 *Build. Environ.* **125** 273 – 284
[18] Jacob J and Sagaut P 2018 *Build. Environ.* **139** 110 – 124
[19] Rullaud S, Blondel F and Cathelain M 2018 *J. Phys.: Conf. Series* **1037** 022023
[20] Sørensen J N and Shen W Z 2002 *J. Fluids Eng.* **124** 393–399
[21] Martínez-Tossas L A, Churchfield M J and Leonardi S 2015 *Wind Energy* **18** 1047–1060
[22] Troldborg N, Zahle F, Réthoré P E and Sørensen N N 2015 *Wind Energy* **18** 1239–1250
[23] Bhatnagar P, Gross E and Krook M 1954 *Phys. Rev.* **94**(3) 511–525
[24] He X and Luo L S 1997 *J. Stat. Phys.* **88** 927–944
[25] Lallemand P and Luo L S 2000 *Phys. Rev. E* **61**(6) 6546–6562
[26] d'Humières D, Ginzburg I, Krafczyk M, Lallemand P and Luo L S 2002 *Philos. Trans. R. Soc. London, A* **360** 437–451
[27] Ginzburg I, Verhaeghe F and d'Humières D 2008 *Commun. Comput. Phys.* **3** 427–478
[28] Geier M, Schönherr M, Pasquali A and Krafczyk M 2015 *Comput. Math. Appl.* **70** 507–547
[29] Geier M, Pasquali A and Schönherr M 2017 *J. Comput. Phys.* **348** 889 – 898
[30] Geier M, Pasquali A and Schönherr M 2017 *J. Comput. Phys.* **348** 862–888
[31] Kutscher K, Geier M and Krafczyk M 2018 *Comput. Fluids* **In Press**
[32] Krafczyk M, Tölke J and Luo L S 2003 *Int. J. Mod. Phys. B* **17** 33–39
[33] Premnath K N, Pattison M J and Banerjee S 2009 *Physica A* **388** 2640–2658
[34] Far E K, Geier M, Kutscher K and Krafczyk M 2016 *Comput. Fluids* **140** 222 – 231
[35] Gehrke M, Janßen C and Rung T 2017 *Comput. Fluids* **156** 247–263
[36] Sarlak H, Meneveau C and Sørensen J 2015 *Renewable Energy* **77** 386–399
[37] Jonkman J, Butterfield S, Musial W and Scott G 2009 Definition of a 5-MW reference wind turbine for offshore system development Tech. Rep. NREL/TP-500-38060 NREL
[38] Janßen C F, Mierke D, Überrück M, Gralher S and Rung T 2015 *Computation* **3** 354

[39] Michelsen J A 1994 Basis3D—a platform for development of multiblock PDE solvers Tech. Rep. Report AFM 92-05 Technical University of Denmark, DTU
[40] Michelsen J A 1994 Block structured multigrid solution of 2D and 3D elliptic PDE's Tech. Rep. Report AFM 94-06 Technical University of Denmark, DTU
[41] Sørensen N N 1995 *General purpose flow solver applied to flow over hills* Ph.D. thesis Risø National Laboratory, Roskilde, Denmark
[42] Troldborg N 2008 *Actuator Line Modeling of Wind Turbine Wakes* Ph.D. thesis Technical University of Denmark, Department of Mechanical Engineering
[43] Wu Y T and Porté-Agel F 2011 *Boundary Layer Meteorol.* **138** 345–366
[44] Jha P K and Schmitz S 2018 *J. Fluid Mech.* **834**
[45] Filippova O and Hänel D 1998 *Journal of Computational Physics* **147** 219 – 228
[46] Hansen M O 2008 *Aerodynamics of Wind Turbines* (London, UK: Earthscan)
[47] Martínez-Tossas L A, Churchfield M J and Meneveau C 2017 *Wind Energy* **20** 1083–1096
[48] Jha P K, Churchfield M J, Moriarty P J and Schmitz S 2013 *J. Sol. Energy Eng.* **136**
[49] Meyer Forsting A R, Pirrung G R and Ramos-García N 2019 *Wind Energ. Sci. Discuss.* **2019** 1–22
[50] Martínez-Tossas L A, Churchfield M J, Yilmaz A E, Sarlak H, Johnson P L, Sørensen J N, Meyers J and Meneveau C 2018 *J. Renewable Sustainable Energy* **10** 033301
[51] Cavar D, Réthoré P E, Bechmann A, Sørensen N N, Martinez B, Zahle F, Berg J and Kelly M C 2016 *Wind Energ. Sci.* **1** 55
[52] Onodera N, Idomura Y, Ali Y and Shimokawabe T 2018 *Proc. of the The International Conference for High Performance Computing, Networking, Storage, and Analysis, Dallas, USA*